Account

Design of Mesoporous Silica at Low Acid Concentrations in Triblock Copolymer-Butanol-Water Systems

Freddy Kleitz,[†,*] Tae-Wan Kim, and Ryong Ryoo[*]

National Creative Research Initiative Center for Functional Nanomaterials, Department of Chemistry
(School of Molecular Science-BK21), Korea Advanced Institute of Science and Technology, Daejeon 305-701, Korea
[*]E-mail: rryoo@kaist.ac.kr
[†]Department of Chemistry, Université Laval, St Foy, Quebec, G1K 7P4, Canada. [*]E-mail: freddy.kleitz@chm.ulaval.ca
Received July 25, 2005

Assembly of hybrid mesophases through the combination of amphiphilic block copolymers, acting as structure-directing agents, and silicon sources using low acid catalyst concentration regimes is a versatile strategy to produce large quantities of high-quality ordered large-pore mesoporous silicas in a very reproducible manner. Controlling structural and textural properties is proven to be straightforward at low HCl concentrations with the adjustment of synthesis gel composition and the option of adding co-structure-directing molecules. In this account, we illustrate how various types of large-pore mesoporous silica can easily be prepared in high phase purity with tailored pore dimensions and tailored level of framework interconnectivity. Silica mesophases with two-dimensional hexagonal (*p6mm*) and three-dimensional cubic (*Fm$\bar{3}$m*, *Im$\bar{3}$m* and *Ia$\bar{3}$d*) symmetries are generated in aqueous solution by employing HCl concentrations in the range of 0.1–0.5 M and polyalkylene oxide-based triblock copolymers such as Pluronic P123 (EO_{20}-PO_{70}-EO_{20}) and Pluronic F127 (EO_{106}-PO_{70}-EO_{106}). Characterizations by powder X-ray diffraction, nitrogen physisorption, and transmission electron microscopy show that the mesoporous materials all possess high specific surface areas, high pore volumes and readily tunable pore diameters in narrow distribution of sizes ranging from 4 to 12 nm. Furthermore, we discuss our recent advances achieved in order to extend widely the phase domains in which single mesostructures are formed. Emphasis is put on the first synthetic product phase diagrams obtained in SiO_2-triblock copolymer-BuOH-H_2O systems, with tuning amounts of butanol and silica source correspondingly. It is expected that the extended phase domains will allow designed synthesis of mesoporous silicas with targeted characteristics, offering vast prospects for future applications.

Key Words : Nanostructured materials, Mesoporous silica, SBA-15, Pore size control, Cubic mesophase

Introduction

Ordered mesoporous silica materials, disclosed in the early 1990's,[1] exhibit tunable pore size, high surface area and pore volume, ease of surface functionalization and controllable morphology, all these being highly promising properties for numerous applications. Since the initial reports, considerable scientific effort has been focused on the preparation, characterization and application of ordered mesoporous silicas.[2] Perspective of applications are envisioned in fields as diverse as catalysis, separation, selective sorption, pollutant removal, drug delivery and release,

Freddy Kleitz was born in 1972 in Saverne, France. He studied chemistry at the Université Louis Pasteur of Strasbourg, France, before joining in 1998 the group of Prof. Ferdi Schüth at the Max-Planck-Institut (MPI) für Kohlenforschung in Mülheim, Germany. He obtained his Ph. D. in chemistry in 2002 for his work in the area of ordered mesoporous materials. In 2002, he joined the group of Prof. Ryong Ryoo at KAIST, Korea, for undertaking post-doctoral research in the field of nanostructured materials. After returning to the MPI in Mülheim in 2003 as a Max-Planck fellow researcher, he was then appointed in 2005 as assistant-professeur at Université Laval in Québec, Canada. Since 2005, Freddy Kleitz holds the Canada Research Chair in *functional nanostructured materials.*

Tae-Wan Kim was born in 1975 in Busan, Korea. He received his B. S. degree in 2000 from Pusan National University and M. S. in 2003 from KAIST. He is expected to obtain a Ph. D. degree in February,

2006 from KAIST, for his work in the field of mesoporous materials in Prof. Ryong Ryoo's group.

Ryong Ryoo was born in 1955 in Hwaseong, Korea. He received his B. S. degree from Seoul Nation University in 1977, and M. S. from KAIST in 1979. He obtained a Ph. D. degree from Stanford University in 1986, for his work on Pt clusters in zeolite cages. After doing a postdoctoral research on solid-state NMR for 1 year at Lawrence Berkeley Laboratory, he returned to KAIST as an assistant professor. He is taking his current position as a chemistry professor at KAIST and director of the Center for Functional Nanomaterials. His research interest is in synthesis and characterization of nanostructured materials including mesoporous materials. He received a number of prizes and awards including 'Research of Future Award' at 2001-ACS Symposium on Nanotechnology in Catalysis, '2002 Academic Award' from Korean Chemical Society, and 'Korea's Top Scientist Award' from Korean government in 2005.

optics, electronics, and many others.[2] It has now become increasingly evident that any design of functional mesoporous materials requires high level of understanding of the factors governing supramolecular assembly at the mesoscale, particularly the formation and growth of hybrid inorganic-organic mesophases, and precise knowledge on the relationship between structure and properties. Detailed control of the structural and textural characteristics such as pore topology, pore diameter, and pore connectivity is desirable to reach the ultimate goals of industrial and commercial applications.

Particularly versatile for the design of large-pore mesoporous materials is the use of nonionic block copolymer-based amphiphiles as structure-directors.[3] In general, syntheses employing nonionic structuring-directing-agents (SDA) are carried out under acidic or neutral conditions and the hybrid inorganic-organic mesophase assembly is governed by weak van der Waals interactions or hydrogen bondings. The first synthesis of mesoporous silica using self-assembly of nonionic surfactant molecules was reported in 1995 by Pinnavaia and co-workers who employed polyoxyethylene-based oligomeric amphiphiles to direct the formation of MSU-type silica materials.[4] Subsequently, Stucky and coworkers[5,6] reported the use of polyalkylene oxide-based triblock copolymers for the preparation of various large-pore silicas, which were represented by the mesoporous silica denoted SBA-15 having 2-dimensional (2-D) hexagonal *p6mm* symmetry. These syntheses were based on the use of organic silica sources such as tetraethoxysilane (TEOS) or tetramethoxysilane (TMOS) in combination with diluted acidic aqueous solution of Pluronic-type triblock copolymer ($< 5-7$ wt% in water) such as P123 (EO_{20}-PO_{70}-EO_{20}, EO = ethylene oxide, PO = propylene oxide) and F127 (EO_{106}-PO_{70}-EO_{106}). In general, the mesoporous silicas obtained with triblock copolymers possess uniform large-pores with dimensions above 5 nm in diameter and thick walls, the latter providing high thermal stability and improved hydrothermal stability compared with mesoporous silicas synthesized with low molecular weight ionic surfactants.[7,8] Mesoporous silicas were also obtained from solutions containing pre-formed liquid crystalline mesophases, at high block copolymer concentrations (> 20 wt%). These syntheses follow the so-called true-liquid crystal template mechanism (TLCT)[9] and will not be discussed in the present account.

Initially, SBA-15 was thought to be more or less a large-pore equivalent of MCM-41 mesoporous silica exhibiting unconnected mesoporous cylindrical channels. MCM-41 is commonly synthesized at alkaline pH with cationic alkylammonium halide surfactants.[1] However, shortly after, the preparation of inverse carbon and platinum replicas of the SBA-15 framework proved that the main mesopore channels of SBA-15 are actually interconnected through a complementary porosity located inside the silica walls.[10] The established presence of complementary porosity in the walls of SBA-15-type silicas is one of the fundamental differences with small pore MCM-41-type silicas, and it is of major importance for further development of block-

copolymer-directed silicas. With regard to this, several groups have precisely investigated the origin and the nature of this complementary porosity and tried to determine whether possibilities for control and tailoring do exist.[10,11] Due to appealing textural and structural properties of block-copolymer-based silicas for potential applications[12] that require improved materials stability or involve large guest molecules, numerous reports have focused on the synthesis and development of ordered mesoporous silica using triblock copolymers as structure-directing agents. Extensive works have been reported on synthesis conditions,[5,6,13-18] mechanisms of formation,[19,20] processes of template removal,[21-23] control of morphology,[24] preparation of periodic organic-inorganic mesoporous hybrids,[25] use of cheap silica sources,[18,26-28] and creation of new phases.[13,29,30] Furthermore, a highly promising field of applications of mesoporous SBA-15-type silicas is their use as hosts or hard templates according the nanocasting pathway to synthesize nanostructured materials[31] and ordered mesoporous carbons.[31g,32]

Aggregation behavior of triblock copolymers, well-described under thermodynamic equilibrium conditions, is known to not only depend on the block copolymer concentration, but importantly also strongly on temperature.[33] Furthermore, the size, geometry, and curvature of the aggregates formed by these types of amphiphiles in water may be determined by the degree of polymerization of each blocks, the volume fraction of each blocks and the degree of incompatibility between the blocks.[3] Therefore, it should be in principle possible to operate a fine tuning of the properties of the resulting hybrid mesophase, considering the concentration and temperature ranges, and choosing carefully the structure directors. Already in the early reports, Stucky and coworkers demonstrated that the ratio of hydrophilic to hydrophobic blocks can determine the structure of the mesophase, with block copolymers that possess longer hydrophilic chains, such as F127, leading to materials having highly curved cage-like pores.[5,6] Later on, Alfredsson *et al.* investigated in details the effects of the length of different block lengths and their relative volume fraction in the synthesis of mesoporous silicas in order to be able to tune pore dimensions and structure of the materials.[34] Zhao and coworkers[15] reported the synthesis of large cage silica material using a different triblock copolymer denoted B50-6600 (EO_{39}-BO_{47}-EO_{39}). This large cage-type mesoporous silica, designated as FDU-1, first reported to have body-centered cubic $Im\bar{3}m$ symmetry, was more recently shown to exhibit the face-centered cubic $Fm\bar{3}m$ structure with intergrowths of 3-D hexagonal phase.[29a] In another example, Chan *et al.*[35] could prepare mesoporous silica with the cubic $Ia\bar{3}d$ phase using a laboratory designed block copolymer functioning as the SDA. Several other authors also reported on the effects of tuning reaction conditions,[11,13c,29] such as synthesis mixture compositions and reaction temperature, on the physicochemical properties of the mesoporous materials. Similarly, Kim *et al.* showed recently in a comprehensive study that it is possible to tailor cage dimensions and pore

opening of SBA-16 silicas by employing copolymer blends jointly with a control of the synthesis temperature and time.[36] Another method of interest is the use of additives to modify the phase behavior of the mesoporous materials. Electrolytes addition was shown to be a possible means of affecting the phase behavior of block copolymer based-mesoporous silicas. Generally, inorganic salts have a strong influence on the copolymer micelles. Salting-out electrolytes (*lyotropic ions*) such as KCl, NaCl or K_2SO_4, which are not adsorbed in the copolymer micelles, dehydrate the hydrophilic portion of the copolymer inducing a pronounced decrease in the preferential interfacial curvature of the micelles. On the other hand, salting-in electrolytes (*hydrotropic ions*) adsorbed in the micelles tend to inhibit growth of the micelles and could increase the preferential interfacial curvature.[37,38] Yu *et al.* used first the salting-out effects caused by the addition of electrolytes in combination with triblock copolymers to generate various mesophase structures with well-defined morphology.[24,39,40] Differently, the salting-in effect observed upon addition of NaI was employed successfully to prepare large-pore cubic $Ia\bar{3}d$ silica.[41] In the case of salt additions, it is important to note that not only the aggregation behavior of copolymer micelles is affected, but the presence of electrolytes will influence hydrolysis and condensation, and the kinetics of aggregation of the silica precursors as well. Finally, success in modifying the mesophase behavior and introducing simultaneously organic functional group was achieved by performing co-condensation reactions involving TEOS and organo-alkoxysilanes for example. Particularly remarkable, are the recently reported syntheses of the large-pore cubic $Ia\bar{3}d$ phase by the co-condensation reaction of TEOS and sulfur-containing silane derivatives,[30,42,43] or a vinyl-containing silane in the presence of NaCl.[38]

Structural and textural control is especially important for the design of functional porous solids for applications involving selectively tuned adsorption and diffusion, and host-guest interactions within elaborated nanostructured materials. However, synthetically, most of these large-pore mesoporous silicas were prepared at high acid catalyst concentrations, around 1.5–2 M in water, under which the mesophase formation occurs through a kinetically controlled competitive assembly of organic and inorganic species into nanostructured domains. The fast kinetics of hydrolysis and condensation of silica at high acid concentrations result in a rapid hybrid mesophase assembly, which somehow limits the possibilities of true and detailed design of textural and structural properties. Co-condensation reaction kinetics are especially difficult to control with this respect. In addition, under high HCl concentrations, only a narrower range of SiO_2/triblock copolymer ratio is acceptable for synthesis, otherwise marked decrease in ordering occurs. In order to overcome problems linked to fast condensation and too rapid mesophase assembly, we have developped an alternative synthetic strategy based on the combined decrease of the acid catalyst concentration and adjusted gel composition ratio, to facilitate modulation of the structural parameters of

the mesostructured products.[44] By this way, we believe that the formation of mesophase can be governed more thermodynamically as the HCl concentration decreases, preventing sudden inter-micellar condensation of silica.

In the following, we will discuss our recent advances regarding the synthesis of high quality large-pore mesoporous silicas with tailored structure and porosity. We will illustrate how various types of large-pore mesoporous silica can easily be prepared in high phase purity with tailored pore dimensions and tailored level of framework interconnectivity. Silica mesophases with 2-D hexagonal (*p6mm*) and 3-D cubic ($Fm\bar{3}m$, $Im\bar{3}m$, and $Ia\bar{3}d$) symmetries are generated in aqueous solution by employing HCl concentrations in the range of 0.1–0.5 M and polyalkylene oxide-based triblock copolymers such as Pluronic P123 (EO_{20}-PO_{70}-EO_{20}) and Pluronic F127 (EO_{106}-PO_{70}-EO_{106}). Moreover, we present our recent advances achieved in order to extend the phase domains in which single mesostructures are formed. Emphasis is put on the first synthetic product phase diagrams obtained in SiO_2-triblock copolymer-BuOH-H_2O systems, with tuning amounts of butanol and silica source correspondingly.

Synthesis of Ordered Mesoporous Silica Using P123 Triblock Copolymer

2-D hexagonal ordered SBA-15 mesoporous silica. An important aspect of SBA-15 is linked to the commercial requirements for the material synthesis, with the need of low cost processes, the possibility of scaling-up the batch size and high yields.[26] Furthermore, it was suggested that all 2-D hexagonally ordered mesoporous silicas templated by polymers containing poly(ethylene oxide) blocks (EO_n) exhibit additional micropores and/or interconnected pores irrespective the conditions used for the synthesis.[45] The formation of this complementary porosity was explained as a result of the penetration of poly(ethylene oxide) blocks of the triblock copolymer in the silicate pore walls of the as-synthesized SBA-15. A precise synthetic control of the wall complementary porosity of SBA-15 is a major challenge in the synthesis of this type of materials. In relation to this, a recent study based on platinum replication and gas adsorption evidenced the influence of the synthesis temperature, with a non-bridging microporosity shown inside the framework walls of SBA-15 samples synthesized at low temperatures (between 308 K and 333 K), while a larger connecting porosity is observed at higher temperature hydrothermal treatment.[46] In the case described by the authors, the change in framework connectivity seems to be related to dehydration of the hydrophilic EO head group with increasing reaction temperature. In another study, it was shown that calcination treatments performed at high temperatures above 1223 K seem to eliminate the complementary porosity,[11] leading to materials with adsorption properties comparable to MCM-41. However, such high temperature calcinations generally lead to a substantial decrease in pore size and appreciable loss of mesoscopic
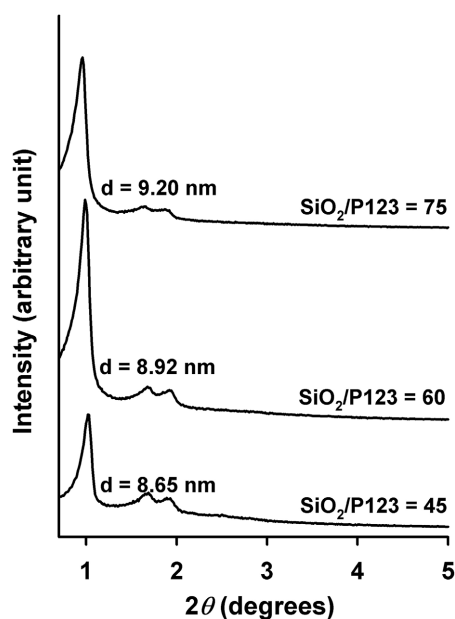
Figure 1. Powder X-ray diffraction patterns obtained for calcined SBA-15 samples synthesized with sodium silicate (5% in water) and initial $SiO_2/P123 = 45$, 60, and 75 (Rigaku Multiplex, operated at 2 kW, using $CuK\alpha$ radiation). Reproduced with permission from ref. 44.

ordering.

In 2003, we proposed a new synthetic approach allowing an highly reproducible control of the network connectivity and wall thickness of SBA-15,[44] by adjusting the $SiO_2/P123$ ratio and decreasing substantially the HCl concentration compared to the original system.[5,6] The new synthesis conditions could be easily tuned to allow combination of

control of the texture and production of high-quality SBA-15 materials, irrespective the synthesis batch size or the nature of the silicon source. In the modified conditions, the acid concentration was sufficiently lowered and the reaction mixture could be well stirred. The synthesis procedure gives high yields of highly ordered mesoporous silica (close to 100% on the basis of silica recovery). Figure 1 shows powder X-ray diffraction patterns for three representative samples, synthesized with sodium silicate as the silica source with $SiO_2/P123$ molar ratios = 45, 60, and 75, respectively, under the same acid concentration. Similar results could be obtained when TEOS for example is used as the silica source. As can be seen, a well-resolved 2-D hexagonal phase is obtained in all cases, with the first diffraction peaks indexed as (10), (11), and (20), being characteristic of hexagonal *p6mm* symmetry. Differences are observed for the *d*-spacing values and the relative distribution of the diffraction peak intensities, suggesting changes in the ratios of pore wall thickness to pore size, and most likely, an increase of the wall thickness with increasing $SiO_2/P123$ molar ratios.[47] The N_2 sorption isotherms are in all cases type IV isotherms with a H1 hysteresis loop and a pronounced capillary condensation step at high relative pressure, characteristic of high-quality large-pore SBA-15 with narrow pore size distributions. Our investigations proved that pore size, pore volume, and BET specific surface areas are decreasing with increasing initial $SiO_2/P123$ ratios. Noteworthily, the pore walls are systematically becoming thicker with increasing $SiO_2/P123$, signifying that our synthesis method allows an effective and simple control the pore wall thickness of SBA-15. The nature of the different network connectivity was ascertained by TEM
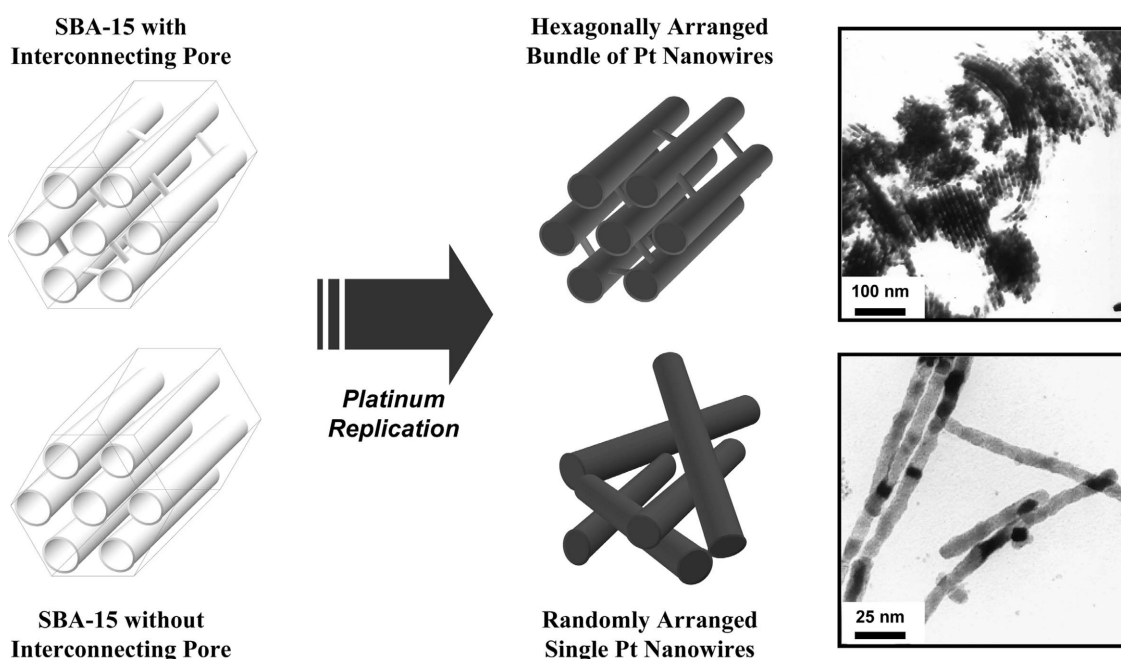
Figure 2. Schematic representation of the framework structure of SBA-15 and replication to platinum nanostructures, with TEM images of the platinum replicas of SBA-15 synthesized with different initial $SiO_2/P123 = 45$ (top right) and 75 (bottom right). Reproduced with permission from ref. 44.

imaging of platinum replicas prepared inside the pores of SBA-15 and isolated after silica etching with diluted HF. Connections between the main channels of SBA-15 could be visualized as bridges between platinum nanowires (see Figure 2). Bridged self-standing platinum networks are obtained at $SiO_2/P123 = 45$, implying full network connectivity of the mesoporous silica. In contrast, no self-standing bundles of connected nanowires are seen for the SBA-15 sample synthesized with $SiO_2/P123 = 75$. Instead, isolated long nanowires or their self-agglomeration was observed. On the basis of replication method with platinum, we concluded that high quality SBA-15 with connected pore channels is produced at low $SiO_2/P123$ ratio, whereas large-pore MCM-41 analogues seem to be generated at higher $SiO_2/P123$. The $SiO_2/P123$ ratio seems to be the main factor affecting the degree of connectivity of the SBA-15 silica. It is likely that the favored interactions between higher amounts of silicate species and the hydrated PEO chains of P123 through hydrogen bondings could cause the decrease of pore connectivity at high silicate concentrations, as the inter-micellar PEO-PEO interactions between adjacent micelles is reduced. Under the conditions described, practically all the silica source is utilized to create the mesophase, irrespective the initial amount of silica precursor. However, in the case of sodium silicate precursor, the presence of NaCl generated *in situ* during neutralization of sodium silicate might also play a role in the degree of framework connectivity. Under our synthesis conditions, it is likely that the walls of the other SBA-15 synthesized at high $SiO_2/P123$ ratios still contain a complementary microporosity, which is, however, non-interconnecting, similarly to previous SBA-15 synthesized at 333 K.[46]

Figure 3 shows the nitrogen adsorption-desorption isotherms and pore size distribution curves, respectively, for series of SBA-15 materials synthesized with increasing temperature of hydrothermal treatment. The sorption isotherms for the different calcined samples all remain well-resolved type IV isotherms, with a sharp capillary condensation step indicative of mesopores narrowly distributed in size, irrespective of the temperature. The shift of the capillary condensation step to higher relative pressure with increasing temperature evidences an increase in the mesopore size, as also indicated by the evolving pore size distribution curves. The pore volumes increase sensibly with increasing temperature and the pore sizes range from 4.5 nm to 13 nm. Our synthesis method clearly permits a systematic and simple control of the pore dimensions of SBA-15 silica, with increasing the aging temperature. Moreover, the new synthesis conditions allow large scaling-up of the synthesis batch and are highly cost-effective since the concentration of acid is reduced and cheap silica source, sodium-silicate, can be employed. The controlled preparation of SBA-15 is the first example showing that the low acid condition affords a precise reproducible control of the interplay between silica polymerization and mesophase assembly, much more thermodynamically than before.

Large-pore Cubic *Ia$\bar{3}$d* ordered KIT-6 mesoporous
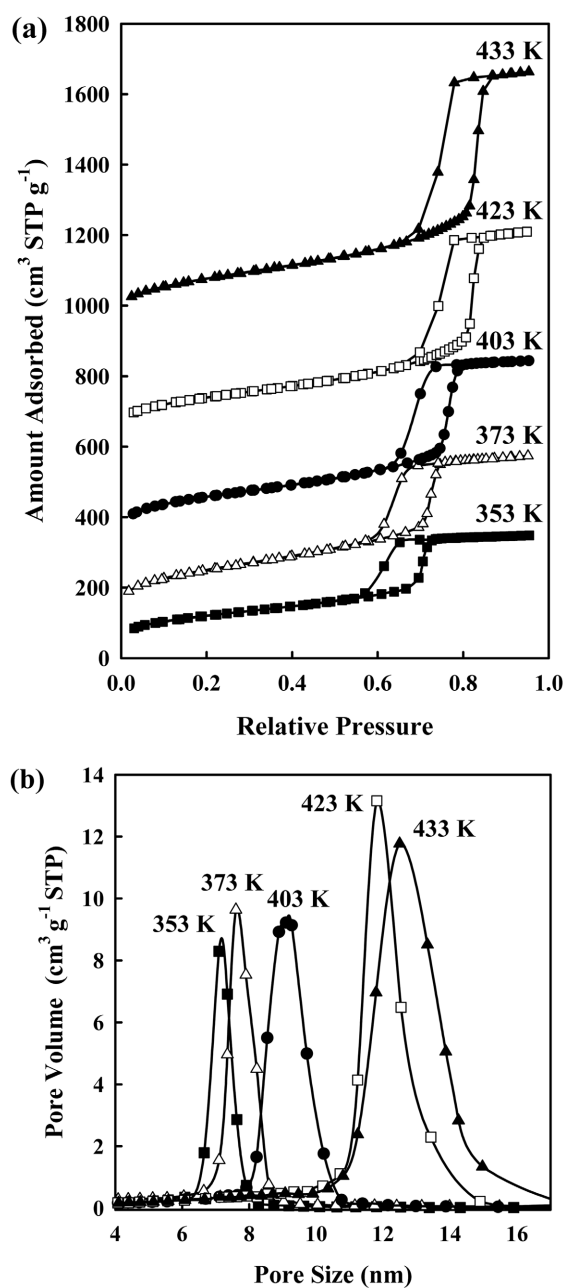
Figure 3. (a) Nitrogen adsorption-desorption isotherms for the hydrothermally treated SBA-15 samples with various temperatures. The isotherms for 373, 403, 423, and 433 K samples are offset vertically by 100, 310, 620, and 940 cm^3 STP g^{-1}, respectively and (b) pore size distributions calculated from the nitrogen adsorption isotherms for the samples with various temperatures by the BJH method.

silica. As mentioned above, the results of the synthesis of SBA-15 showed that synthesis of mesoporous silica at low acid concentrations can be operated in a more controlled manner than syntheses performed under high concentrations (1.5–2 M), because of a more delicate balance between the kinetic factors and thermodynamic effects. We have discovered that the simple principle of balancing kinetic and thermodynamic effects is a general way to improve considerably the materials synthesis processes. Using the low acid

concentration method, we have been able to tune the phase behavior of the silica mesophase precisely to synthesize MCM-48-like large-pore mesoporous silica, which we have designated as KIT-6, with the cubic $Ia\bar{3}d$ structural symmetry.[48,49] To achieve this, we used the phase-controlling (*thermodynamic*) effect of addition of butanol in the SiO_2-P123-H_2O-HCl system and the micelle-folding (*kinetic*) effect during silica species polymerization simultaneously.[8] Under these conditions, the phase behavior of the triblock copolymer in the presence of silica species can be enriched in water since slower silica condensation kinetic allows the use of polar organic additives acting as co-surfactants to modify *almost thermodynamically* the mesophase behavior. Compared to procedures reported by others,[30,38,41-43] this synthesis has now the advantages of allowing fine tuning of uniform pore diameters over a wide range of pore sizes (4–12 nm), tailoring of the framework interconnectivity, high reproducibility in large quantity, and the cost-effective aspect of lower amounts of acid and cheap sodium-silicate silica source. We discovered that the addition of butanol as a *co-solute*[50] and low HCl concentrations are the prerequisite to obtain the desired cubic $Ia\bar{3}d$ phase. It turned out that the cubic $Ia\bar{3}d$ phase is formed in the presence of butanol
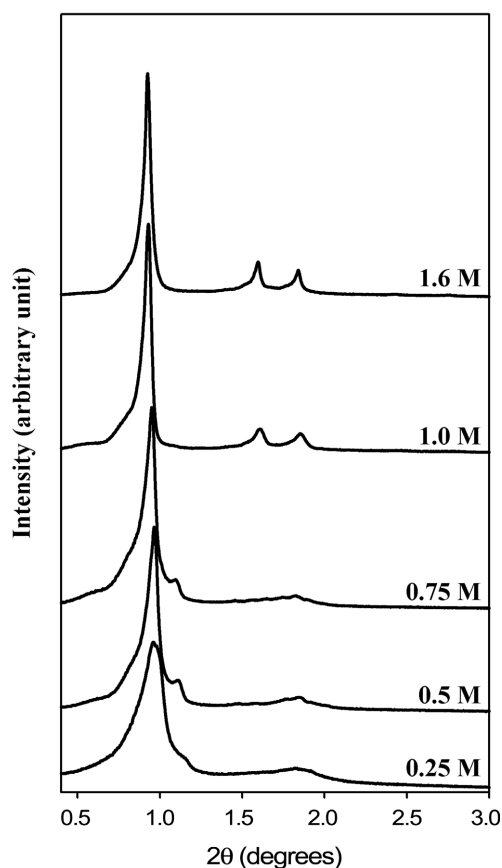
Figure 4. High resolution powder XRD (HRXRD) patterns for the mesostructured silica materials obtained using 0.017 P123:1.2 TEOS:1.31 BuOH:*x* HCl:195 H_2O. The molar ratio of HCl (*x*) was varied to *x* = 0.915, 1.83, 2.75, 3.66, and 5.856 giving [HCl] = 0.25, 0.50, 0.75, 1.0 and 1.6, respectively. Reproduced with permission from ref. 49.

exclusively if the concentration of the acid catalyst is decreased to as low as 0.75 M. Powder XRD patterns of calcined mesoporous silicas synthesized with different HCl concentrations in the range of 0.25–2.0 M are depicted in Figure 4, illustrating the major role of the HCl concentration on the structure of the mesophase. The exact assignment to the bicontinuous cubic $Ia\bar{3}d$ symmetry was confirmed by TEM and electron crystallography investigations.[51] The unit cell size, calculated from the (211) reflection of the $Ia\bar{3}d$ phase, is measured to be 22.5 nm for a calcined material obtained at 373 K and at 0.5 M and with TEOS/BuOH = 1.2/1.31, a value much larger than that of MCM-48.[1] The sorption isotherm obtained for the cubic phase is a type IV isotherm characteristic of high-quality large-pore mesoporous materials, with a H1 hysteresis loop indicating channel-like pores and narrow pore size distribution. The isotherm is very similar to the ones obtained for 2-D hexagonal SBA-15 silicas. The cubic material synthesized at 373 K has a high BET surface area in the range 700–800 m^2 g^{-1} and pore volume around 1 cm^3 g^{-1}. The $Ia\bar{3}d$ phase can be generated with various range of compositions at low HCl concentrations in the presence of butanol. The median pore diameter of materials synthesized at 373 K varies between 6.8 and 8.2 nm, strongly depending on the initial gel composition. It is also worth mentioning that with the present synthesis method, the cubic $Ia\bar{3}d$ KIT-6 silica can easily be synthesized with sodium silicate used as silica source instead of TEOS. Furthermore, tailoring of the textural parameters of the cubic $Ia\bar{3}d$ KIT-6 silica was achieved by varying the hydrothermal treatment between 308–403 K, similarly to SBA-15. Figure 5 shows the nitrogen sorption isotherms and pore size distributions, respectively, for a selected starting gel composition (0.017 P123/1.2 TEOS/1.31 BuOH/1.83 HCl/195 H_2O). As it can be seen, the sorption isotherms remain type IV isotherms, with retention of the narrow distribution of pore size, irrespective of the temperature. Depending on the starting composition, pore sizes up to 12 nm can be obtained for materials when subjected to hydrothermal treatment at temperatures above 393 K.[48] Moreover, the nature of the pore interconnectivity of the large-pore cubic $Ia\bar{3}d$ silica materials was analyzed by using both the inverse platinum and carbon replication methods.[48,49] Thus, the CMK-type carbon replicas were synthesized using a series of cubic mesoporous silicas prepared at temperatures ranging from 308 to 403 K, with sucrose as the carbon precursor, and characterized by powder XRD. As illustrated in Figure 6, the structural symmetry of the cubic $Ia\bar{3}d$ KIT-6 template was preserved after carbon replication when KIT-6 was prepared with aging temperatures above 343 K, whereas structurally-transformed mesoporous carbon structures similar to CMK-1[52] could be produced using KIT-6 templates synthesized at temperatures ranging from 308 to 333 K. The structure transformation is determined from the presence of the additional reflection below 0.7° 2 *theta* angle. It can be concluded that the two enantiomeric interpenetrating channel networks forming the gyroid structure are independent
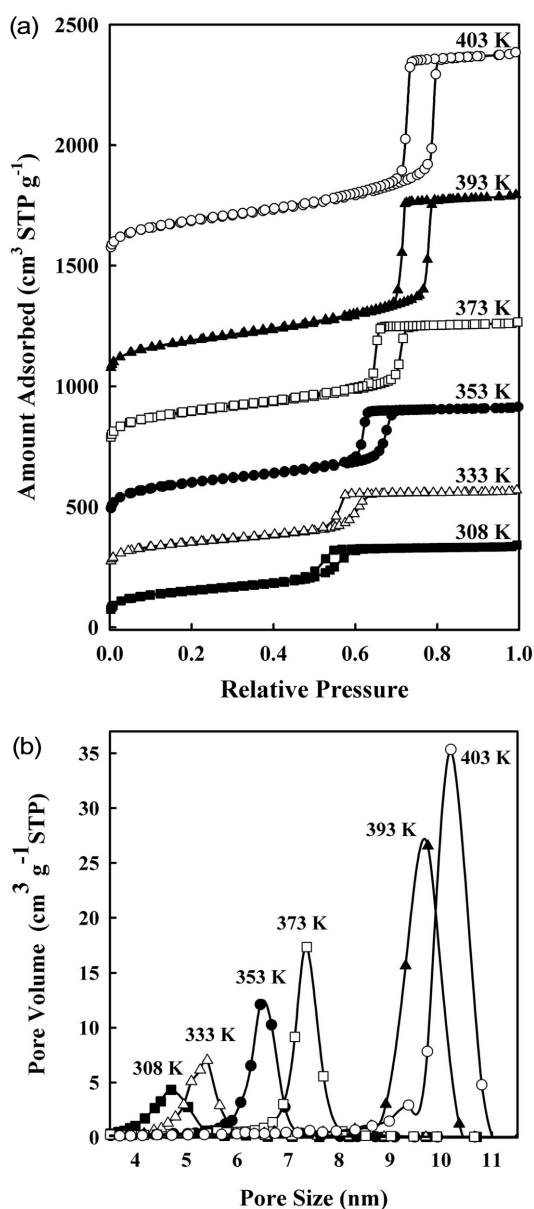
Figure 5. (a) N_2 adsorption-desorption isotherms for cubic $Ia\bar{3}d$ KIT-6 silica samples synthesized at different hydrothermal treatment temperatures, with the composition 0.017 P123:1.2 TEOS: 1.31 BuOH:1.83 HCl:195 H_2O. The isotherms for 333, 353, 373, 393 and 403 K are offset vertically by 200, 400, 700, 1000, and 1500 cm^3 STP g^{-1}, respectively and (b) pore size distributions of the samples. The pore size was analyzed with the adsorption branch using the BJH algorithm. Reproduced with permission from ref. 49.

from each other in the case of KIT-6 materials synthesized at temperatures ranging between 308–333 K. At higher treatment temperatures, faithful inverse carbon replicas are produced. We attributed this feature to the presence of porous bridges or connectivity between the two subsystems of mesoporous channels. This network interconnectivity was confirmed directly by imaging platinum replicas synthesized in the $Ia\bar{3}d$ silica materials prepared at 373 K.[48]

We examined the processes linked to the formation of the cubic phase by collecting XRD patterns at different stages
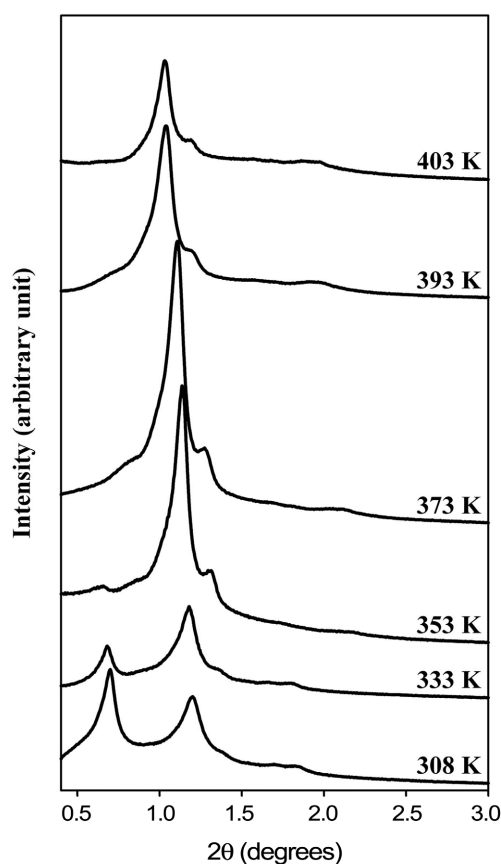
Figure 6. HRXRD patterns for cubic mesoporous carbon replicas with rod-type nanostructures prepared from cubic $Ia\bar{3}d$ KIT-6 mesoporous silicas synthesized at different temperatures. Reproduced with permission from ref. 49.

during the reaction. The time-resolved XRD measurements, depicted in Figure 7, revealed that the cubic $Ia\bar{3}d$ phase was formed *via* a structural evolution mechanism. Accordingly, the mechanism seems to involve a transformation from a lamellar phase, appearing initially after 4–6 h of reaction depending on starting mixture composition, to the desired bicontinuous cubic phase. Butanol is known to act as a co-surfactant in the block copolymer-water systems, which co-micellizes with the block copolymer, determining the micellar interfacial curvature. To explain the presence of the lamellar phase and the structural evolution, we proposed that the addition of butanol produces a pronounced decrease in the interfacial curvature of the micellar system. This effect could be rationalized on the account of changes in the hydrophobic to hydrophilic volume ratio of the block copolymer micelles, leading first to formation of a meso-phase with low curvature.[50b,53-55] By slowing down the condensation kinetics, it is likely that the silicates species remain quite '*soft*', and the less rigid silica oligomers allow for more flexibility for reorganizing the structure and adapting changes in curvature. At early stages, silicate species should be loosely condensed with low degree of cross-linking. Upon further reaction at 308 K, condensation increases progressively in the silicate region, which possibly

(a)

(b)   **Lamellar**   **Cubic** *Ia3̄d*
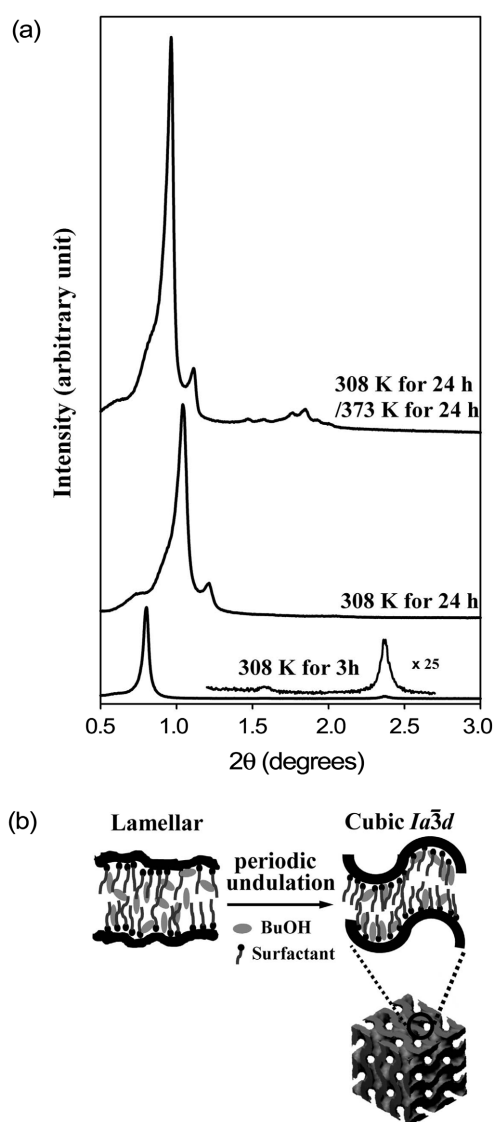
Figure 7. (a) HRXRD patterns for the mesostructure obtained using 0.017 P123: 1.2 TEOS:1.31 BuOH:1.83 HCl:195 H$_2$O during formation of the cubic *Ia 3̄ d* phase, as function of temperature and time. (b) Schematic illustration of the lamellar-to-cubic transformation. Reproduced with permission from ref. 49.

imposes stress and geometrical frustration provoking undulations and regular folding of the silica surface. Anisotropic fluctuations in the hybrid mesophase due to silica condensation will induce significant changes in the inorganic-organic interfacial curvature, and the subsequent observed change in symmetry leading ultimately to the gyroid infinite periodic minimal surface (IPMS).

This approach that we proposed to add butanol to the copolymer system appears as an elegant alternative strategy for the synthesis of large-pore cubic *Ia 3̄ d* mesoporous silicas, compared to other methods based on the use of salt additions, time-consuming synthesis of new structuring-directing entities or kinetically dependent co-condensation reactions.

Synthesis of Large-pore Cage-like Face-centered-cubic *Fm 3̄ m* Mesoporous Silica with Adjustment of the HCl Concentration

Ordered mesoporous materials with cage-like pores and interconnected 3-D porous framework are suggested to be superior to hexagonal structures with one-dimensional channels when dealing with applications involving selectively tuned diffusion, immobilization of large molecules, or host-guest interactions. Furthermore, materials such as 2-D hexagonal SBA-15 are already available as model systems for adsorption and diffusion studies in cylindrical pores, while there is still a need for ideal model systems of spherical cavities. With respect to this, our group has reported a synthesis route to prepare highly ordered 3-D large-cage mesoporous silica, designated as KIT-5, with cubic *Fm 3̄ m* close-packed structure. The synthesis uses uniquely TEOS with F127 triblock copolymer in aqueous solution at low HCl concentration regime.[56] The N$_2$ adsorption-desorption isotherm (Figure 8a) obtained for calcined mesoporous KIT-5 silica is a type IV with broad H2 hysteresis loop that is indicative of large uniform cage-like pores.[57] Due to the fact that conventional methods of pore size analysis assuming cylindrical pore channels, such as the BJH method,[58] are not appropriate for cage-like structures, we decided to employ a geometrical method described by Ravikovitch *et al.*[57] to evaluate more accurately the pore dimensions. Typical KIT-5 silica synthesized at 373 K has a BET surface area of 715 m^2 g^{-1}, total pore volume of 0.45 cm^3 g^{-1} and a cavity diameter of about 8–9 nm. Hydrothermal treatments at various temperatures ranging from 318 to 423 K enabled a really effective tailoring of not only the mesopore diameters, but also the pore aperture size. In the case of this cubic phase, the exact structure determination was crucial and the assignment to *Fm 3̄ m* symmetry was confirmed by the combined analysis of the powder XRD patterns and TEM images. Highly resolved low-angle diffraction peaks could be indexed to the face-centered cubic (*fcc*) *Fm 3̄ m* symmetry lattice (Figure 8b), and no additional reflections related to 3-D hexagonal intergrowths were observed. The excellent 3-D cubic mesoscopic order of KIT-5 was also evidenced by TEM (Figure 9). It is important to remark that the images taken along the [110] direction revealed no intergrowths with 3-D hexagonal phase, which are often reported to occur for other cage-like mesoporous silicas (SBA-2, SBA-12, and FDU-1).[59] This particular feature gives additional evidence for the purity of this cubic *Fm 3̄ m* phase. The presence of the "*twined*" hexagonal close packed structure was ruled out, since the Fourier diffractograms corresponding to the images taken along [110] showed no stacking faults.

The new porous structure can be viewed as a compact cubic close packing of globular cage-like pores, with the exact nature of the interconnectivity of the cages remaining to be determined. The aqueous synthesis route to achieve highly ordered cubic *Fm 3̄ m* mesoporous silica is based on

Design of Mesoporous Silica at Low Acid Concentrations

Bull. Korean Chem. Soc. **2005**, Vol. 26, No. 11   1661
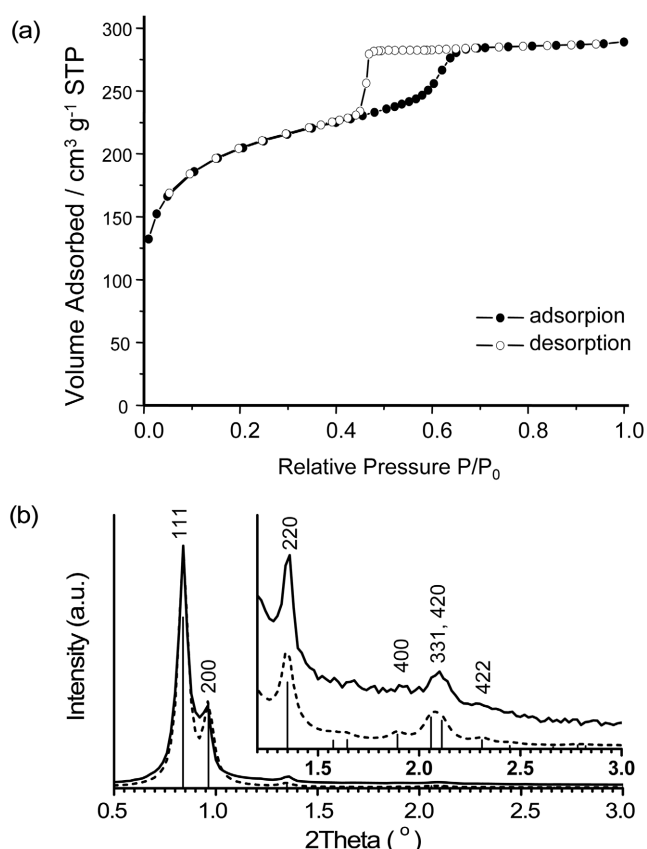
Figure 8. Nitrogen physisorption isotherm of cubic $Fm\bar{3}m$ KIT-5 mesoporous silica synthesized at 35 °C followed by aging at 100 °C. (b) Experimental (solid line) and simulated (dashed line) HRXRD profiles obtained for the same KIT-5 sample. Reproduced with permission from ref. 56.

Figure 9. TEM image viewed from [110] direction. The inset shows respective Fourier diffractogram. Reproduced with permission from ref. 56.

the use of F127 triblock copolymer ($EO_{106}PO_{70}EO_{106}$), which exhibits high hydrophilic to hydrophobic volume ratio (high EO/PO) implying high curvature of the micelles, in dilute acidic conditions. The decrease in the mesophase formation kinetics by reducing the concentration of HCl is thought here to be most appropriate for the optimized cooperative assembly of highly curved micelles and silicates into well-ordered close-packed micellar cubic structure. Differently, Fan *et al.*[21] suggested a synthesis method toward a large cage-like mesoporous silica with *fcc* symmetry, with high HCl concentrations. However, this synthetic method is complicated, involving the addition of salt combined with trimethylbenzene and long hydrothermal reaction time (3 days). Further, the assignment made to a $Fm\bar{3}m$ structure may be discutable due to poorly resolved XRD patterns and lack of comprehensive TEM analysis. Jaroniec *et al.* recently applied successfully the concept of decreasing the acid concentration to prepare high quality FDU-1 materials using additionally salting-out effects of NaCl added to the solution.[60] This new preparation method led to FDU-1 that has about twice the pore volume and a much narrower pore size distribution compared to the values observed for previously obtained cage-like FDU-1. It should be mentioned that mesoporous silica with *fcc* structure exists as well in smaller

pore systems. For example, previous efforts by Sakamoto *et al.*[61] led to the preparation of a phase-pure cubic $Fm\bar{3}m$ mesoporous organo-functionalized silica with small pore diameter (< 4 nm). Very recently also, Anwander and coworkers reported a small-pore equivalent of the KIT-5 phase exhibiting organic groups located inside the silica walls. This small pore KIT-5 exhibits very well-resolved XRD pattern commensurate with the $Fm\bar{3}m$ symmetry.[62]

Phase Domains of Large-pore Ordered Mesoporous Silica

Mesoporous silica in the EO_{20}-PO_{70}-EO_{20}-butanol-H_2O ternary system. In most of the works described so far in the literature, the synthesis of highly ordered mesoporous silicas using triblock copolymers was successful within a rather narrow range of synthesis mixture composition. Especially, cubic phases are often obtained in narrow compositional range, even sometimes at a single composition point, with the materials being very different if the ratios of reactants are only slightly modified. In section 2, we have first demonstrated that SBA-15 is readily obtainable with wider range of silicon source to copolymer ratios if the acid concentration is decreased substantially to values below 0.5 M. It is therefore likely that the compositional ranges suitable for the other phases, which we developed specifically at low acid concentrations, could as well be widely extended. Indeed, we discovered that the cubic $Ia\bar{3}d$ phase domain is considerably extended when tuning the amounts of butanol and silica source correspondingly at HCl concentrations as low as 0.5 M.[49] At present, the range where the cubic $Ia\bar{3}d$ phase is generated, is widely enlarged compared to our initial report on the synthesis.[48] In fact, the amount of butanol necessary for the formation of the $Ia\bar{3}d$ phase is highly depending on the initial reagents ratio. By changing
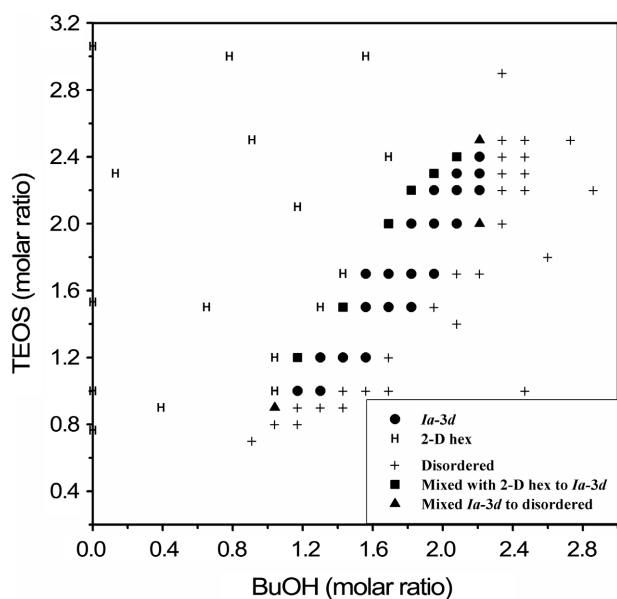
Figure 10. Synthetic product phase diagram of mesophase structures established according to the XRD measurements. Each sample is prepared with a molar ratio of 0.017 P123:x TEOS:y BuOH:1.83 HCl:195 H_2O. Reproduced with permission from ref. 49.

simultaneously these two synthetic variables, we have been able to map the phases that can be generated in the systems, resulting in a synthesis product phase diagram as a function of the amounts of silica source and BuOH. The synthesis product phase diagram of mesoporous silica in the EO_{20}-PO_{70}-EO_{20}-Butanol-H_2O ternary system is shown in Figure 10. For this phase diagram, all syntheses were performed at a reaction temperature of 308 K, and the subsequent aging temperature was 373 K. As it can be seen, the region where the cubic $Ia\bar{3}d$ phase is obtained is situated between a large region of 2-D hexagonal mesophase and a region where a less ordered phase is produced. The interval ratios where the $Ia\bar{3}d$ phase forms are P123/TEOS/BuOH = 0.017/1.0–2.4/1.2–2.2 in molar ratio. At a fixed amount of TEOS, increasing amounts of BuOH added to the synthesis batch lead to transition from 2-D hexagonal to the cubic $Ia\bar{3}d$ mesophase, to, finally, the disordered phase, through smaller domains of intermediate mixed phases. These features are

illustrated by XRD for a fixed ratio P123/TEOS/BuOH = 0.017/1.5/y, where y is varied from 1.31 to 1.97 at 0.5 M HCl. The XRD patterns recorded as a function of the BuOH amount showed that the structure evolves from a 2-D hexagonal phase to the cubic $Ia\bar{3}d$ phase as the amount of butanol is increased.[49] Conversely, increasing the amount of the silica source in the system while keeping the BuOH amount constant, leads to transition from the poorly ordered phase, to well-ordered $Ia\bar{3}d$ phase to, finally, the 2-D hexagonal phase. At high BuOH content ($y > 2.2$ in mole ratio), only poorly ordered materials are formed, irrespective of the amount of TEOS. Low BuOH content yields materials with the 2-D hexagonal phase. In Table 1 are summarized the lattice and textural parameters of these representative cubic $Ia\bar{3}d$ porous mesostructured materials. Nitrogen adsorption-desorption isotherms were measured on cubic $Ia\bar{3}d$ samples synthesized according to the gel compositions taken in the cubic phase domain. The sorption isotherms, depicted in Figures 11b, are all type IV isotherms with the pronounced capillary condensation step. As shown in Table 1, an observed trend is the decrease of the mesopore size as the quantities of TEOS and BuOH are increased. Increasing TEOS/P123 ratio is expected to lead to thicker framework walls, similarly to what was observed for SBA-15.[44] However, only slight changes in wall thickness are estimated, most likely as a consequence of the presence of butanol. The synthetic product phase diagram, which we proposed, is the first diagram of this type obtained in the SiO_2-EO_{20}-PO_{70}-EO_{20}-alcohol-H_2O system, and can be envisioned as a starting point for more designed preparation of large-pore mesoporous silicas in general.

Mesoporous silica in the EO_{106}-PO_{70}-EO_{106}-Butanol-H_2O ternary system.

Transformation of mesoporous silica from cubic $Fm\bar{3}m$, to cubic $Im\bar{3}m$, to 2-D hexagonal $p6mm$ symmetry: Following the discovery of the face-centered cubic KIT-5 silica phase, we subsequently explored the effects of the addition of an organic additive such as butanol in the SiO_2-EO_{106}-PO_{70}-EO_{106}-H_2O system, searching for the possibility of mesophase transformation. In the system studied, the butanol/triblock copolymer mass ratio only was utilized to direct specifically the formation of high quality silica meso-

Table 1. Structural parameters of the cubic $Ia\bar{3}d$ mesoporous silicas were prepared at the molar ratio of 0.017 P123: x TEOS:y BuOH:1.83 HCl:195 H_2O. Reproduced with permission from ref. 49

$[x, y]$	a (nm)	S_{BET} ($m^2 g^{-1}$)	S_{DFT} ($m^2 g^{-1}$)	V_t ($cm^3 g^{-1}$)	V_{DFT} ($cm^3 g^{-1}$)	w_{BJHads} (nm)	w_{DFT} (nm)	d_s (nm)
[1.0, 1.31][†]	22.7	784	724	0.94	0.92	8.2	8.1	3.2
[1.2, 1.44]	22.4	725	683	0.93	0.91	7.6	7.9	3.3
[1.5, 1.70]	22.4	753	704	0.92	0.91	7.3	7.6	3.6
[2.0, 2.03]	22.4	753	699	0.82	0.82	6.4	7.1	4.2
[2.4, 2.22]	21.6	778	704	0.83	0.81	6.1	6.8	4.0

a is the XRD unit cell parameter equals to $6^{1/2}d_{211}$; S_{BET}, apparent BET specific surface area deduced from the isotherm analysis in the relative pressure range from 0.05 to 0.20; V_t, total pore volume at relative pressure 0.95; w_{BJH}, the pore diameter calculated using the BJH method. S_{DFT}, specific surface area, V_{DFT}, total pore volume and w_{DFT}, mesopore diameter, calculated by DFT method using the kernel of NLDFT equilibrium capillary condensation isotherms of N_2 at 77 K on silica. d_s, is the wall thickness evaluated by geometrical model: $d_s = a/2$-w_{DFT}, (ref. 52c) [†]Sample synthesized following the conditions reported initially, with P123 : BuOH = 1 : 1 (wt%) (ref. 48).
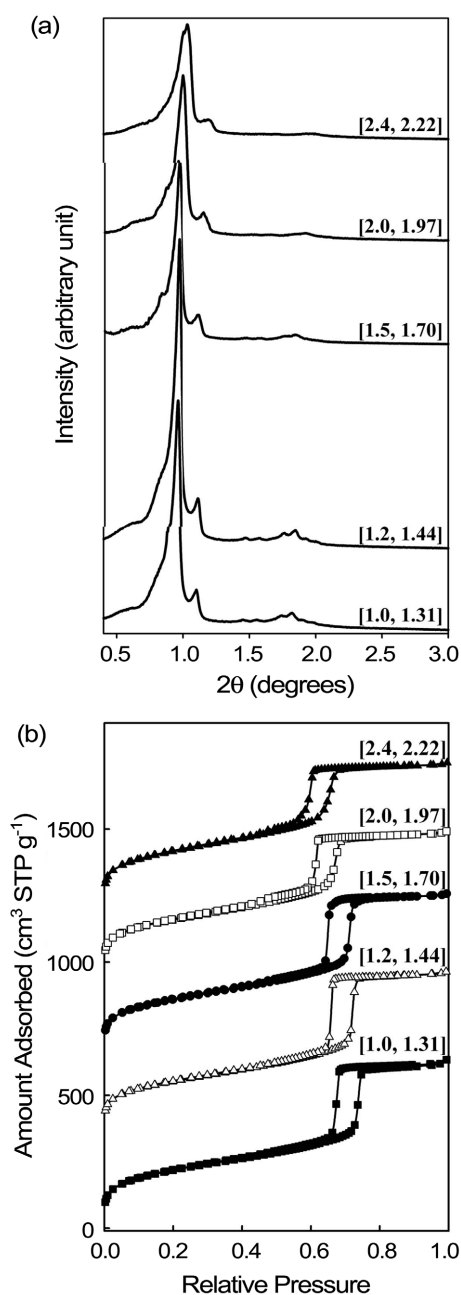
Figure 11. (a) HRXRD patterns for the cubic mesoporous KIT-6 silicas. Each sample was prepared as the molar ratio of 0.017 P123: x TEOS:y BuOH:1.83 HCl:195 H_2O, where [x, y] was as shown, and (b) N_2 adsorption-desorption isotherms. The isotherms for [1.2, 1.44], [1.5, 1.70], [2.0, 1.97] and [2.4, 2.22] are offset vertically by 350, 650, 950, and 1200 cm^3 STP g^{-1}, respectively. Reproduced with permission from ref. 49.

phases with cubic $Fm\overline{3}m$, cubic $Im\overline{3}m$ or 2-D hexagonal $p6mm$ structures, with all other synthetic parameters and molar ratios remaining constant.[63] We showed that the structural evolutions were exclusively due to the addition of different amounts of BuOH as the unique phase-controlling agent. Phase transitions from $fcc\ Fm\overline{3}m$, to body-centered cubic (bcc) $Im\overline{3}m$ to, finally, 2-D hexagonal $p6mm$ mesostructures accompanied with the pore widening and opening were observed upon increasing the amount of BuOH. In this
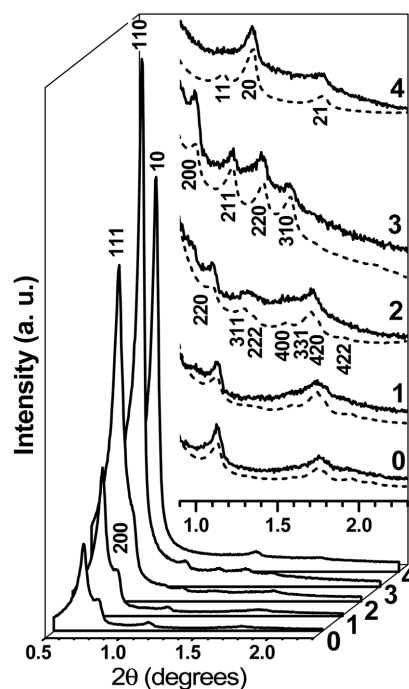
Figure 12. Experimental (solid line) and simulated (dashed line) XRD powder patterns of samples with mass ratio BuOH:F127 = 0, 1, 2, 3, and 4. Reproduced with permission from ref. 63.

case also, the lattice type and the symmetry of the mesoporous materials could be accurately determined with the help of combining comprehensive XRD and TEM investigations. The powder XRD patterns of the samples as-synthesized with different amounts of butanol are shown in Figure 12. In the absence of butanol, the diffraction peaks are indexed to a lattice with $fcc\ Fm\overline{3}m$ symmetry. As we discussed above, this silica consists of large cage-like pores or cavities arranged in a cubic close-packed mesostructure.[56] Addition of amounts of butanol to the starting mixture up to BuOH : F127 = 2 (in molar ratio) does not alter the symmetry of the mesophase, but clear differences in relative intensities of the diffraction peaks are observed. At BuOH : F127 = 3, a transition to the $bcc\ Im\overline{3}m$ symmetry occurred, the material being hence analogous to SBA-16.[13] This was also confirmed for the calcined sample by type IV nitrogen physisorption isotherm with a broad H2 hysteresis loop indicative of the uniform cage-like pores.[57] A further increase in the amount of butanol added (up to BuOH : F127 = 4) induced the formation of "*a near to 2-D hexagonal*" SBA-15-type structure. We speculated that the evolution of the mesophase from the cage-like fcc and bcc to the near-cylindrical 2-D hexagonal pore structure may originate from changes in the interfacial curvature and the hydrophobic to hydrophilic volume fractions. Similar transition between $Im\overline{3}m$ and $p6mm$ phases resulting from the reduced hydration of the polar head groups and lowering curvature exists, for example, in a polyalkylene oxide-based surfactant-water system where, besides, an epitaxial relationship between both phases was evidenced.[64] In our case, it is likely that the curvature of the micellar aggregates could be reduced due to
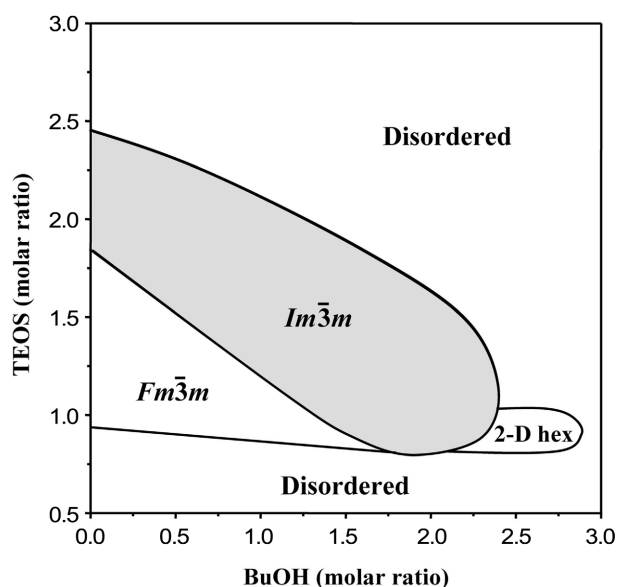
Figure 13. Synthetic product phase diagram of mesophase structures established according to the XRD measurements. Each sample is prepared with a molar ratio of 0.0035 F127:x TEOS:y BuOH:0.91 HCl:117 H_2O.

a decrease in hydration of the polyethylene oxide groups caused by higher amounts of butanol. In addition, the location of butanol at the hydrophilic-hydrophobic interface may be responsible for a shift of the silica region in the micelles, which resulted in reducing the silica wall thickness. These results are very significant since they highlight the systematic control over the formation of mesoporous silica with tailored pore architecture, by employing structural evolutions induced by the addition of different amounts of butanol as a mesophase-controlling agent.

Description of the phase domains of mesoporous silica in EO_{106}-PO_{70}-EO_{106}-Butanol-H_2O: In Figure 13 is depicted the first synthesis phase diagram of mesostructured silica in the EO_{106}-PO_{70}-EO_{106}-Butanol-H_2O system obtained at 0.5 M HCl.[65] Silica mesophase formed at 318 K followed by treatment at 373 K for 24 hours are represented as a function of the initial amounts of BuOH and TEOS. Similarly to the previous diagram of the product phases, mesoporous silica products are characterized from preparations with simultaneous increase of TEOS and BuOH quantities added to the reaction mixtures. The first observation that can be made is that large domains of the diagram correspond either to the *bcc* $Im\bar{3}m$ phase or to some disordered materials. Irrespective of the amounts of BuOH added ($0 \le y \le 3.0$), disordered materials are formed for low values of TEOS ratios below 0.8 or high values above 2.3 in molar ratio. In the remaining part of the diagram ($0.75 < x < 2.3$), the $Im\bar{3}m$ phase is the dominating phase generated in the EO_{106}-PO_{70}-EO_{106}-Butanol-H_2O system. It is noteworthy that at a fixed TEOS ratio $1.75 \le x \le 2.25$, the $Im\bar{3}m$ phase is formed in the absence of BuOH. Increasing amounts of the co-surfactant, in this chosen interval of TEOS content produce a transition from the well-developed $Im\bar{3}m$ phase to the disordered

phase. We observed that with decreasing amounts of TEOS from x = 2.25 to 1.75, the BuOH quantity needed to induce this transition to the disordered phase progressively increases from y = 0.75 to as high as y = 2.25 in molar ratio. In the interval of TEOS within $0.8 \le x < 1.75$, the phase behavior is enriched with the presence of a region of the *fcc* $Fm\bar{3}m$ mesophase visible for low BuOH amounts. A very small domain of a 2-D hexagonal phase exists at high value of BuOH ($y > 2.25$) and exclusively low TEOS values ($0.8 < x < 1.0$). Most importantly, in this range of TEOS ($0.8 \le x \le 1.75$), the $Im\bar{3}m$ phase is formed only in the presence of butanol. The amount of BuOH needed to induce the phase transition from $Fm\bar{3}m$ to $Im\bar{3}m$ is also shown to be higher for lower TEOS amounts. The quantities of butanol required reach values as high as y = 1.75, for low TEOS values (x close to 0.8). In contrast to the phase behavior of mesoporous SiO_2 in EO_{20}-PO_{70}-EO_{20}-Butanol-H_2O, increasing the amount of the silica source in the system while keeping the BuOH amount constant does not lead to only one possible sequence of phase transitions, but the type of transition is highly depending on the amount of BuOH chosen to be included in the mixture. At low BuOH ($y \le 1.5$), increasing the TEOS amount results in a *disorder-fcc-bcc-disorder* transition sequence. At medium BuOH content ($1.5 < y \le 2.25$), increasing TEOS leads to a *disorder-bcc-disorder* sequence. At high BuOH amounts ($y > 2.25$), transitions following a *disorder-hexagonal-bcc-disorder* sequence occur and, at the highest values of BuOH, a
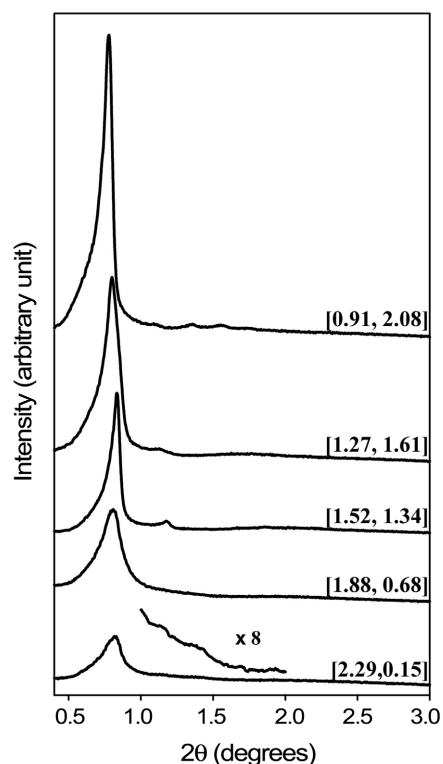
Figure 14. HRXRD patterns for the cubic $Im\bar{3}m$ SBA-16-type mesoporous silicas. Each sample was prepared as the molar ratio of 0.0035 F127:x TEOS:y BuOH:0.91 HCl:117 H_2O, where [x, y] was as shown.
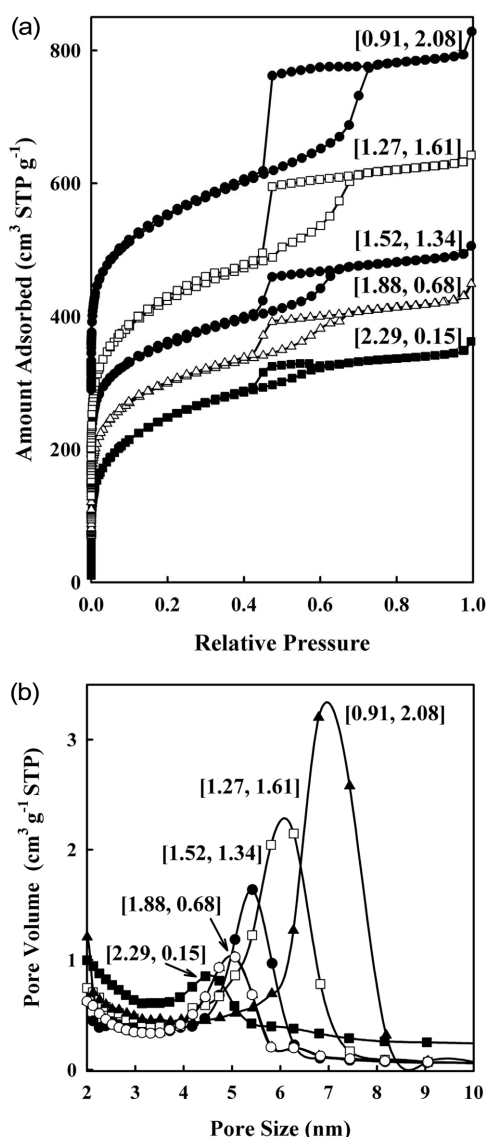
Figure 15. (a) N2 adsorption-desorption isotherms for cubic $Im\bar{3}m$ silica samples. Each sample was prepared as the molar ratio of 0.0035 F127:x TEOS:y BuOH:0.91 HCl:117 H_2O, where [x, y] was varied as shown. The isotherms for [1.88, 0.68], [1.52, 1.34], [1.27, 1.61], and [0.91, 2.08] samples are offset vertically by 60, 130, 130, and 280 cm^3 STP g^{-1}, respectively and (b) pore size distributions of the samples. The pore size distribution for [2.29, 0.15] sample is offset vertically by 0.2 $cm^3 g^{-1}$ STP.

disorder-hexagonal-disorder sequence occurs. In conclusion, the silica mesophase behavior phase seems more complex in the EO_{106}-PO_{70}-EO_{106}-Butanol-H_2O system, and therefore, this work may be paving the way for the preparation of a rich diversity of material physicochemical properties.

Synthesis of SBA-16 in the EO_{106}-PO_{70}-EO_{106}-Butanol-H_2O system: Other methods are available for the preparation of cubic $Im\bar{3}m$ SBA-16 silica, in the absence of co-surfactant such as butanol.[5,6,13,16,36] Nevertheless, our investigations revealed that the structural properties of the cubic $Im\bar{3}m$ mesoporous silicas can be tailored efficiently at low HCl concentrations by adjusting the amounts of the silica

source and co-surfactant, and the hydrothermal treatment temperature. Figure 14 represents the XRD patterns of various mesoporous silica samples obtained in the *bcc* region of the synthetic products phase diagram with different values of TEOS and BuOH. All diffraction patterns can be indexed to the $Im\bar{3}m$ phase, with however, clear differences in the position of the diffraction peaks and their intensity distributions with changing the ratios x and y for the synthesis. These changes in the diffractograms suggest differences in structural parameters, such as wall thickness and pore dimensions. Currently, detailed structural investigations accompanied with modeling of the XRD patterns are still needed to substantiate precisely the observed evolution of the diffractograms. Figure 15 shows the N_2 adsorption-desorption isotherms and respective pore size distributions for the same series of cubic mesoporous silicas synthesized according to the gel compositions with different amounts of the BuOH and TEOS. All N_2 isotherms measured are type IV isotherms with a H2-type adsorption-desorption hysteresis characteristic of mesoporous materials with cage-like pores.[57] A pronounced increase of the mesopore volume is observed with combined decrease of the TEOS amount and increase of the butanol content. The largest mesopore volume and adsorption capacity are measured for the sample synthesized with $x = 0.91$ and $y = 2.08$, whereas, the minimum adsorption capacity is measured for $x = 2.29$ and low amounts of butanol ($y = 0.15$). This behavior is also reflected on the dimension of the cage as illustrated by the evolution of the pore size distribution (Figure 15b). The structural parameters of cubic $Im\bar{3}m$ mesostructured silica materials synthesized with the addition of TEOS and BuOH are summarized in Table 2. As observed, the pore size (measured with a geometrical model[27,57]) increases monotonously with concurrent increase of butanol and decrease of TEOS employed. The mesopore diameter and primary mesopore volume of the samples have a linear relationship with the increasing content of BuOH. At the present stage, however, we can not state conclusively whether the role of butanol is only to act as a co-surfactant for the phase

Table 2. Structural parameters of the cubic $Im\bar{3}m$ mesoporous silicas which were prepared at the molar ratio of 0.0035 F127: x TEOS:y BuOH:0.87 HCl:117 H_2O

[x, y]	a (nm)	S_{BET} ($m^2 g^{-1}$)	S_{ex} ($m^2 g^{-1}$)	V_t ($cm^3 g^{-1}$)	V_{mi} ($cm^3 g^{-1}$)	V_p ($cm^3 g^{-1}$)	w_d (nm)
[2.29, 0.15]	15.3	890	30	0.53	0.22	0.27	9.9
[1.88, 0.68]	15.5	860	40	0.56	0.21	0.30	10.3
[1.52, 1.34]	15.1	810	30	0.56	0.18	0.34	10.5
[1.27, 1.61]	15.6	1050	30	0.77	0.24	0.50	11.5
[0.91, 2.08]	16.2	980	30	0.79	0.19	0.56	12.3

a is the XRD unit cell parameter equals to $2^{1/2}d_{110}$; S_{BET}, apparent BET specific surface area deduced from the isotherm analysis in the relative pressure range from 0.05 to 0.20; V_t, total pore volume at relative pressure 0.95; V_{mi}, micropore volume, V_p, primary mesopore volume, which were estimated from nitrogen adsorption data using the α_s-plot method (Jaroniec, M.; Kruk, M.; Oliver, J. P. *Langmuir* **1999**, *15*, 5410); w_d, the primary mesopore cage diameter calculated using the equation for a cubic structure with spherical cavities (refs. 29, 57).

(a)

(b)
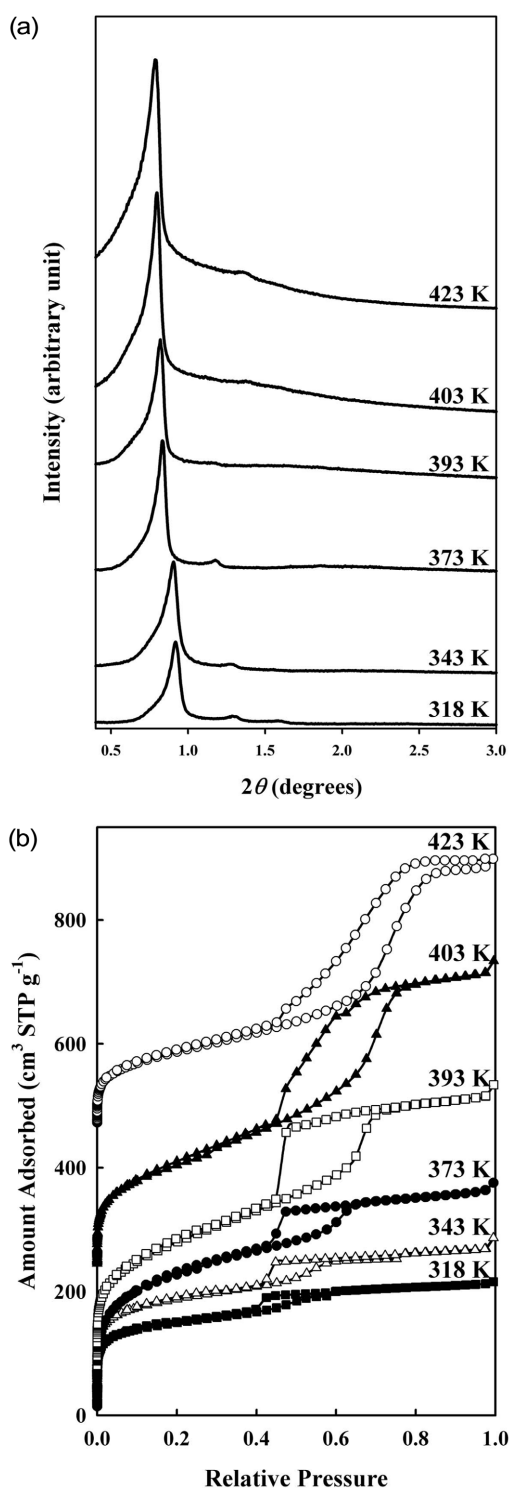
Figure 16. (a) HRXRD patterns for cubic $Im\bar{3}m$ silica samples synthesized using 0.0035 F127:1.52 TEOS:1.34 BuOH:0.91 HCl:117 H_2O with various hydrothermal treatment temperatures and (b) nitrogen adsorption-desorption isotherms. The isotherms for 343 K, 393 K, 403 K, and 423 K samples are offset vertically by 30, 80, 240, and 470 cm^3 STP g^{-1}, respectively.

formation, or to act as well as a pore expander producing larger cage dimensions. This is one of the aspects which remain to be clarified by additional investigations. In addi-

Table 3. Effects of hydrothermal treatment on the structure of cubic $Im\bar{3}m$ mesoporous silicas

T (K)	a (nm)	S_{BET} ($m^2\,g^{-1}$)	S_{ex} ($m^2\,g^{-1}$)	V_t ($cm^3\,g^{-1}$)	V_{mi} ($cm^3\,g^{-1}$)	V_p ($cm^3\,g^{-1}$)	w_d (nm)
318	13.6	510	10	0.33	0.13	0.17	8.2
343	13.9	550	20	0.38	0.12	0.21	8.8
373	15.1	810	30	0.56	0.18	0.34	10.5
393	15.3	730	40	0.67	0.03	0.59	12.4
403	15.7	600	40	0.73	~0	0.66	13.0
423	16.1	420	30	0.64	~0	0.61	13.1

T, temperature, at which the reaction mixture was aged for 24 h after synthesis at 318 K, at the molar ratios of 0.0035 F127:1.52 TEOS:1.34 BuOH:0.87 HCl:117 H_2O; see Table 2 for other notations.

tion, we have studied the effect of the hydrothermal treatment temperature on the $Im\bar{3}m$ phase. The XRD patterns recorded on the materials synthesized at different treatment temperatures are depicted in Figure 16a. The increase of the hydrothermal treatment temperature caused the displacement of the XRD reflections toward lower 2 theta angles, which provided evidence of an increase in the unit-cell parameter (see Table 3). Variation of the hydrothermal treatment temperatures between 318 and 423 K results in a progressive augmentation in nitrogen sorption capacity, mesopore volume and pore size. The shape of N_2 isotherms of silica samples prepared at temperatures up to 393 K remain unchanged exhibiting a hysteresis corresponding to cage-type ink-bottle pores (Figure 16b). With higher heating temperatures above 393 K, the isotherms obtained are shown to evolve towards curves with narrower hysteresis feature suggesting opening of the pore windows and the formation of more cylindrical-like pore structure.

Conclusions

The synthesis conditions for the preparation of large-pore ordered mesoporous silicas were highly optimized through our insights into the kinetically controlled assembly of organic and inorganic species. The synthesis routes using P123 or F127 triblock copolymers as structure-directing-agents and BuOH as a co-agent under low acid conditions allow the formation of great variety of mesostructures, which have 2-D hexagonal $p6mm$, cubic $Ia\bar{3}d$, cubic $Fm\bar{3}m$ or cubic $Im\bar{3}m$ symmetry. The synthesis conditions that we have developped (low concentrations of HCl, possibility of using low-cost sodium silicate, and well mixing of reactants) are shown to be suitable for preparing materials with excellent degree of mesoscopic order, and tunable pore size, wall thickness, and pore connectivity. It is here worth emphasizing that such straightforward tailoring of the phase behavior is made possible under the low HCl concentrations conditions utilized. Furthermore, the introduction of *n*-butanol to a triblock copolymer-based mesoporous silica synthesis offers great possibilities of tuning the material structure. In this regard, it is certainly reasonable to also consider syntheses of mesostructured materials using other organic additives that could directly affect the hydrophilic-

hydrophobic interface of the triblock copolymers aggregates. The extended phase domains that we have developed lead to facile synthesis of ordered mesoporous silica with a more precise structural and textural control over a wide range of physicochemical properties, offering vast prospects for future applications of large-pore silica materials.

Mesoporous silicas with 3-D framework interconnectivity are especially applicable as selective sorbents, catalyst supports, matrices for biomolecules, flow and transport devices, or advanced host-guests systems. In addition, the well-defined porosity and structure render the silica materials suitable as reference materials for adsorption and diffusion studies. Furthermore, the mesoporous silicas that we described in this account are versatile *hard templates* for the preparation of various nanocast non-siliceous materials with interesting textural properties. For example, the cubic $Ia\bar{3}d$ phase was already employed successfully as a template to generate several new highly ordered mesoporous carbon materials, with either rod-like structure as in the case of CMK-8[48,49,51,66] and large-pore CMK-1 analogue,[49] or tube-type structure for material denoted CMK-9.[48,66] In other recent examples, cubic KIT-6 silica was used to manufacture diverse nanostructured porous metal oxide-based materials. Shen *et al.* described the use of KIT-6 as a template for the fabrication of mesoporous RuO_2, which seemed to show interesting catalytic activity for the CO oxidation.[67] Very recently also, mesostructured WO_3 and CeO_2 materials obtained from KIT-6 silica, were reported for gas sensing applications.[68] Finally, we demonstrated in a recent study that large-pore mesoporous silicas with tailored porosity are suitable hosts for the selective adsorption of vinyl monomers for the production of functional polymer nanocoatings on silica walls.[69] In this approach, mesoporous SBA-15 and KIT-6 silicas containing sufficient amount of complementary pores in their framework walls were employed to create new types of highly porous and fully integrated functional polymer-inorganic nanocomposites. We can certainly expect in the near future further developments in the synthesis, utilizations and applications of ordered mesoporous silica prepared under the '*almost thermodynamically*' favored conditions that we have achieved by reducing the acid catalyst concentrations.

References

 1. (a) Kresge, C. T.; Leonowicz, M. E.; Roth, W. J.; Vartuli, J. C.; Beck, J. S. *Nature* **1992**, *359*, 710. (b) Beck, J. S.; Vartuli, J. C.; Roth, W. J.; Leonowicz, M. E.; Kresge, C. T.; Schmitt, K. D.; Chu, C. T.-W.; Olson, D. H.; Sheppard, E. W.; McCullen, S. B.; Higgins, J. B.; Schenkler, J. L. *J. Am. Chem. Soc.* **1992**, *114*, 10834.

 2. (a) Ciesla, U.; Schüth, F. *Microporous Mesoporous Mater.* **1999**, *27*, 131. (b) Ying, J. Y.; Mehnert, C. P.; Wong, M. S. *Angew. Chem. Int. Ed. Engl.* **1999**, *38*, 56. (c) Schüth, F. *Chem. Mater.* **2001**, *13*, 3184. (d) Scott, B. J.; Wirnsberger, G.; Stucky, G. D. *Chem. Mater.* **2001**, *13*, 3140. (e) Schmidt, W.; Schüth, F. *Adv. Mater.* **2002**, *14*, 629. (f) Stein, A. *Adv. Mater.* **2003**, *15*, 763. (g) Soler-Illia, G. J. A. A.; Patarin, J.; Lebeau, B.; Sanchez, C. *Chem. Rev.* **2002**, *102*, 4093. (h) Sanchez, C.; Soler-Illia, G. J. A. A.; Ribot, F.; Grosso, D. S *C. R. Chimie* **2003**, *6*, 1131. (i) Taguchi, A.; Schüth, F. *Microporous Mesoporous Mater.* **2005**, *77*, 1.

 3. Soler-Illia, G. J. A. A.; Crepaldi, E. L.; Grosso, D.; Sanchez, C. *Curr. Opin. Colloid Interface Sci.* **2003**, *8*, 109, and references therein.

 4. Bagshaw, S. A.; Prouzet, E.; Pinnavaia, T. *Science* **1995**, *269*, 1242.

 5. Zhao, D.; Feng, J.; Huo, Q.; Melosh, N. ; Fredrickson, G. H.; Chmelka, B. F.; Stucky, G. D. *Science* **1998**, *279*, 548.

 6. Zhao, D.; Huo, Q.; Feng, J.; Chmelka, B. F.; Stucky, G. D. *J. Am. Chem. Soc.* **1998**, *120*, 6024.

 7. Cassiers, K.; Linssen, T.; Mathieu, M.; Benjelloun, M.; Schrijnemakers, K.; Van der Voort, P.; Cool, P.; Vansant, E. F. *Chem. Mater.* **2002**, *14*, 2317.

 8. Kruk, M.; Celer, E. B.; Jaroniec, M. *Chem. Mater.* **2004**, *16*, 698.

 9. Attard, G. S.; Glyde, J. C.; Goltner, C. G. *Nature* **1995**, *378*, 366.

10. (a) Ryoo, R.; Ko, C. H.; Kruk, M.; Antoschuk, V.; Jaroniec, M. *J. Phys. Chem. B* **2000**, *104*, 11465. (b) Jun, S.; Joo, S. H.; Ryoo, R.; Kruk, M.; Jaroniec, M.; Liu, Z.; Ohsuna, T.; Terasaki, O. *J. Am. Chem. Soc.* **2000**, *122*, 10712. (c) Shin, H. J.; Ko, C. H.; Ryoo, R. *J. Mater. Chem.* **2001**, *11*, 260.

11. (a) Imperor-Clerck, M.; Davidson, P.; Davidson, A. *J. Am. Chem. Soc.* **2000**, *12*, 898. (b) Miyazawa, K.; Inagaki, S. *Chem. Commun.* **2000**, 2121. (c) Shin, H. J.; Ryoo, R.; Kruk, M.; Jaroniec, M. *Chem. Commun.* **2001**, 349. (d) Ravikovitch, P. L.; Neimark, A. V. *J. Phys. Chem. B* **2001**, *105*, 6817. (e) Matos, J. R.; Mercuri, L. P.; Kruk, M.; Jaroniec, M. *Chem. Mater.* **2001**, *13*, 1726. (f) Goltner, C. G.; Smarsly, B.; Berton, B.; Antonietti, M. *Chem. Mater.* **2001**, *13*, 1617. (g) Galarneau, A.; Cambon, H.; DiRenzo, F.; Ryoo, R.; Choi, M.; Fajula, F. *New J. Chem.* **2003**, *27*, 73.

12. (a) Kim, S.-W.; Son, S. U.; Lee, S. I.; Hyeon, T.; Chung, Y. K. *J. Am. Chem. Soc.* **2000**, *122*, 1550. (b) Cho, Y. S.; Park, J. C.; Lee, B.; Kim, Y.; Yi, J. *Catal. Lett.* **2002**, *81*, 89. (c) Yang, P.; Wirnsberger, G.; Huang, H. C.; Cordero, S. R.; McGehee, M. D.; Scott, B.; Deng, T.; Whitesides, G. M.; Chmelka, B. F.; Buratto, S. K.; Stucky, G. D. *Science* **2000**, *287*, 465. (d) Wirnsberger, G.; Scott, B.; Chmelka, B. F.; Stucky, G. D. *Adv. Mater.* **2000**, *12*, 1450. (e) Xu, W.; Akins, D. L. *J. Phys. Chem. B* **2002**, *106*, 1991. (f) Zhou, H.-S.; Yamada, T.; Asai, K.; Honma, I.; Uchida, H.; Katsube, T. *Stud. Surf. Sci. Catal.* **2002**, *141*, 623. (g) Washmon-Kriel, L.; Jimenez, V. L.; Balkus, K. J., Jr. *J. Mol. Catal. B: Enzymatic* **2000**, *10*, 453. (h) Yiu, H. H. P.; Wright, P. A.; Botting, N. P. *Microporous Mesoporous Mater.* **2001**, *44-45*, 763. (i) Takahashi, H.; Li, B.; Sasaki, T.; Miyazaki, C.; Kajino, T.; Inagaki, S. *Microporous Mesoporous Mater.* **2001**, *44-45*, 755. (j) Han, Y.-J.; Watson, J. T.; Stucky, G. D.; Butler, A. *J. Mol. Catal. B: Enzymatic* **2002**, *17*, 1. (k) Han, Y.-J.; Stucky, G. D.; Butler, A. *J. Am. Chem. Soc.* **1999**, *121*, 9897.

13. Sakamoto, Y.; Kaneda, M.; Terasaki, O.; Zhao, D.; Kim, J. M.; Stucky, G. D.; Shin, H. J.; Ryoo, R. *Nature* **2000**, *408*, 449.

14. Newalkar, B. L.; Komarneni, S. *Chem. Commun.* **2002**, 1774.

15. Yu, C.; Yu., Y.; Zhao, D. *Chem. Commun.* **2000**, 575.

16. Van der Voort, P.; Benjelloun, M.; Vansant, E. F. *J. Phys. Chem. B* **2002**, *106*, 9027.

17. (a) Schmidt-Winkel, P.; Lukens, W. W., Jr.; Zhao, D.; Yang, P.; Chmelka, B. F.; Stucky, G. D. *J. Am. Chem. Soc.* **1999**, *121*, 254. (b) Lettow, J. S.; Han, Y. J.; Schmidt-Winkel, P.; Yang, P.; Zhao, D.; Stucky, G. D.; Ying, J. Y. *Langmuir* **2002**, *16*, 8291.

18. (a) Kim, S. S.; Pauly, T. R.; Pinnavaia, T. J. *Chem. Commun.* **2000**, 1661. (b) Kim, S. S.; Karkambar, A.; Pinnavaia, T. J.; Kruk, M.; Jaroniec, M. *J. Phys. Chem. B* **2001**, *105*, 7663.

19. (a) Flodström, K.; Teixeira, C. V.; Amenitsch, H.; Alfredsson, V.; Lindén, M. *Langmuir* **2004**, *20*, 4885. (b) Flodström, K.; Wennerström, H.; Alfredsson, V. *Langmuir* **2004**, *20*, 680. (c) Flodström, K.; Wennerström, H.; Teixeira, C. V.; Amenitsch, H.; Lindén, M.; Alfredsson, V. *Langmuir* **2004**, *20*, 10311.

20. (a) Ruthstein, S.; Frydman, V.; Kababya, S.; Goldfarb, D. *J. Phys. Chem. B* **2003**, *107*, 1739. (b) Ruthstein, S.; Frydman, V.; Goldfarb, D. *J. Phys. Chem. B* **2004**, *108*, 9016.

21. Kleitz, F.; Schmidt, W.; Schüth, F. *Microporous Mesoporous Mater.* **2003**, *65*, 1.

22. Tian, B.; Liu, X.; Yu, C.; Gao, F.; Luo, Q.; Xie, S.; Tu, B.; Zhao, D. *Chem. Commun.* **2002**, 1186.

23. Yang, C. M.; Zibrowius, B.; Schmidt, W.; Schüth, F. *Chem. Mater.* **2004**, *16*, 2918.

24. (a) Zhao, D.; Yang, P.; Melosh, N.; Feng, J.; Chmelka, B. F.; Stucky, G. D. *Adv. Mater.* **1998**, *10*, 1380. (b) Yang, P.; Zhao, D.; Chmelka, B. F.; Stucky, G. D. *Chem. Mater.* **1998**, *10*, 2033. (c) Zhao, D.; Sun, J. Y.; Li, Q. Z.; Stucky, G. D. *Chem. Mater.* **2000**, *12*, 275. (d) Feng, P. Y.; Bu, X. H.; Stucky, G. D.; Pine, D. J. *J. Am. Chem. Soc.* **2000**, *122*, 994.

25. (a) Zhu, H.; Jones, D. J.; Zajac, J.; Rozière, J.; Dutartre, R. *Chem. Commun.* **2001**, 2568. (b) Muth, O.; Schellbach, C.; Fröba, M. *Chem. Commun.* **2001**, 2032. (c) Goto, Y.; Inagaki, S. *Chem. Commun.* **2002**, 2410. (d) Guo, W.; Kim, I.; Ha, C. S. *Chem. Commun.* **2003**, 2692.

26. Kim, J. M.; Stucky, G. D. *Chem. Commun.* **2000**, 1159.

27. Matos, J. R.; Mercuri, L. P.; Kruk, M.; Jaroniec, M. *Langmuir* **2002**, *18*, 884.

28. Joo, S. H.; Ryoo, R.; Kruk, M.; Jaroniec, M. *J. Phys. Chem. B* **2002**, *106*, 4640.

29. Matos, J. R.; Kruk, M.; Mercuri, L. P.; Jaroniec, M.; Zhao, L.; Kamiyama, T.; Terasaki, O.; Pinnavaia, T. J.; Liu, Y. *J. Am. Chem. Soc.* **2003**, *125*, 821.

30. Liu, X.; Tian, B.; Yu, C.; Gao, F.; Xie, S.; Tu, B.; Che, R.; Peng, L.-M.; Zhao, D. *Angew. Chem. Int. Ed.* **2002**, *41*, 3876.

31. (a) Shin, H. J.; Ko, C. H.; Ryoo, R. *J. Mater. Chem.* **2001**, *11*, 260. (b) Han, Y.-J.; Kim, J. M.; Stucky, G. D. *Chem. Mater.* **2000**, *12*, 2068. (c) Huang, M. H.; Choudrey, A.; Yang, P. *Chem. Commun.* **2000**, 1063. (d) Yang, H.; Shi, Q.; Tian, B.; Lu, Q.; Gao, F.; Xie, S.; Fan, J.; Yu, C.; Tu, B.; Zhao, D. *J. Am. Chem. Soc.* **2003**, *125*, 4724. (e) Tian, B. Z.; Liu, X. Y.; Yang, H. F.; Xie, S. H.; Yu, C. Z.; Tu, B.; Zhao, D. Y. *Adv. Mater.* **2003**, *15*, 1370. (f) Laha, S.; Ryoo, R. *Chem. Commun.* **2003**, 2138. (g) Schüth, F. *Angew. Chem. Int. Ed.* **2003**, *42*, 3604. (h) Feng, H. F.; Zhao, D. Y. *J. Mater. Chem.* **2005**, *15*, 1217.

32. (a) Jun, S.; Joo, S. H.; Ryoo, R.; Kruk, M.; Jaroniec, M.; Liu, Z.; Ohsuna, T.; Terasaki, O. *J. Am. Chem. Soc.* **2000**, *122*, 10712. (b) Joo, S. H.; Choi, S. J.; Oh, I.; Kwak, J.; Liu, Z.; Terasaki, O.; Ryoo, R. *Nature* **2001**, *412*, 169. (c) Zhang, W.-H.; Liang, C.; Sun, H.; Shen, Z.; Guan, Y.; Ying, P.; Li, C. *Adv. Mater.* **2002**, *14*, 1776. (d) Vix-Guterl, C.; Boulard, S.; Parmentier, J.; Patarin, J.; Werckmann, J. *Chem. Lett.* **2002**, *10*, 1062. (e) Kim, T.-W.; Park, I.-S.; Ryoo, R. *Angew. Chem. Int. Ed.* **2003**, *42*, 4375. (f) Solovyov, L.; Kim, T.-W.; Kleitz, F.; Terasaki, O.; Ryoo, R. *Chem. Mater.* **2004**, *16*, 2274.

33. Alexandridis, P.; Hatton, T. A. *Colloids Surfaces A: Physicochem. Eng. Aspects* **1995**, *96*, 1.

34. (a) Kipkemboi, P.; Fogden, A.; Alfredsson, V.; Flodström, K. *Langmuir* **2001**, *17*, 5398. (b) Flodström, K.; Alfredsson, V. *Microporous Mesoporous Mater.* **2003**, *59*, 167.

35. Chan, Y. T.; Lin, H.-P.; Mou, C. Y.; Liu, S. T. *Chem. Commun.* **2002**, 2878.

36. Kim, T.-W.; Ryoo, R.; Kruk, M.; Gierszal, K. P.; Jaroniec, M.; Kamiya, S.; Terasaki, O. *J. Phys. Chem. B* **2004**, *108*, 11480.

37. Kabalnov, A.; Olsson, U.; Wennerström, H. *J. Phys. Chem.* **1995**, *98*, 6220.

38. Wang, Y. Q.; Yang, C. M.; Zibrowius, B.; Spliethoff, B.; Lindén, M.; Schüth, F. *Chem. Mater.* **2003**, *15*, 5029.

39. (a) Yu, C.; Tian, B.; Fan, J.; Stucky, G. D.; Zhao, D. *Chem. Commun.* **2001**, 2726. (b) Yu, C.; Tian, B.; Fan, J.; Stucky, G. D.; Zhao, D. *J. Am. Chem. Soc.* **2002**, *124*, 4556.

40. Fan, J.; Yu, C.; Gao, F.; Lei, J.; Tian, B.; Wang, L.; Luo, Q.; Tu, B.; Zhou, W.; Zhao, D. *Angew. Chem. Int. Ed.* **2003**, *42*, 3146.

41. Flodström, K.; Alfredsson, V.; Källrot, N. *J. Am. Chem. Soc.* **2003**, *125*, 4402.

42. Tian, B. Z.; Liu, X.; Solovyov, L.; Liu, Z.; Yang, H.; Zhang, Z.; Xie, S.; Zhang, F.; Tu, B.; Yu, C.; Terasaki, O.; Zhao, D. *J. Am. Chem. Soc.* **2003**, *126*, 865.

43. Hodgins, R.; Garcia-Bennet, A.; Wright, P. A. *Microporous Mesoporous Mater.* **2005**, *79*, 241.

44. Choi, M.; Heo, W.; Kleitz, F.; Ryoo, R. *Chem. Commun.* **2003**, 1340.

45. Joo, S. H.; Ryoo, R.; Kruk, M.; Jaroniec, M. *J. Phys. Chem. B* **2002**, *106*, 4640.

46. Galarneau, A.; Cambon, H.; DiRenzo, F.; Ryoo, R.; Choi, M.; Fajula, F. *New J. Chem.* **2003**, *27*, 73.

47. Sauer, J.; Marlow, F.; Schüth, F. *Phys. Chem. Chem. Phys.* **2002**, *3*, 5579.

48. Kleitz, F.; Choi, S. H.; Ryoo, R. *Chem. Commun.* **2003**, 2136.

49. Kim, T.-W.; Kleitz, F.; Paul, B.; Ryoo, R. *J. Am. Chem. Soc.* **2005**, *127*, 7601.

50. (a) Ågren, P.; Lindén, M.; Rosenholm, J. B.; Schwarzenbacher, R.; Kriechbaum, M.; Amenitsch, H.; Laggner, P.; Blanchard, J.; Schüth, F. *J. Phys. Chem. B* **1999**, *103*, 5943. (b) Feng, P.; Bu, X.; Pine, D. J. *Langmuir* **2000**, *16*, 5304. (c) Kleitz, F.; Blanchard, J.; Zibrowius, B.; Schüth, F.; Ågren, P.; Lindén, M. *Langmuir* **2002**, *18*, 4963.

51. Sakamoto, Y.; Kim, T.-W.; Ryoo, R.; Terasaki, O. *Angew. Chem. Int. Ed.* **2004**, *43*, 5231.

52. Ryoo, R.; Joo, S. H.; Jun, S. *J. Phys. Chem. B* **1999**, *103*, 7743. (b) Kaneda, M.; Tsubakiyama, T.; Carlsson, A.; Sakamoto, Y.; Ohsuna, T.; Terasaki, O.; Joo, S. H.; Ryoo, R. *J. Phys. Chem. B* **2002**, *106*, 1256. (c) Solovyov, L. A.; Zaikovskii, V. I.; Shmakov, A. N.; Belousov, O. V.; Ryoo, R. *J. Phys. Chem. B* **2002**, *106*, 12198.

53. Armstrong, J.; Chowdhry, B.; Mitchell, J.; Beezer, A.; Leharne, S. *J. Phys. Chem.* **1996**, *100*, 1738.

54. Kwon, K.-W.; Park, M. J.; Hwang, J.; Char, K. *Polym. J.* **2001**, *33*, 404.

55. (a) Holmqvist, P.; Alexandridis, P.; Lindman, B. *Macromolecules* **1997**, *30*, 6788. (b) Holmqvist, P.; Alexandridis, P.; Lindman, B. *J. Phys. Chem. B* **1998**, *102*, 1149.

56. Kleitz, F.; Liu, D.; Anilkumar, G. M.; Park, I.-S.; Solovyov, L. A.; Shmakov, A. N.; Ryoo, R. *J. Phys. Chem. B* **2003**, *107*, 14296.

57. (a) Ravikovitch, P. I.; Neimark, A. V. *Langmuir* **2002**, *18*, 1550. (b) Ravikovitch, P. I.; Neimark, A. V. *Langmuir* **2002**, *18*, 9830.

58. Barrett, E. P.; Joyner, L. G.; Halenda, P. P. *J. Am. Chem. Soc.* **1951**, *73*, 373.

59. Zhou, W.; Hunter, H. M. A.; Wright, P. A.; Ge, Q.; Thomas, J. M. *J. Phys. Chem. B* **1998**, *102*, 6934.

60. Grudzien, R. M.; Jaroniec, M. *Chem. Commun.* **2005**, 1076.

61. Sakamoto, Y.; Díaz, I.; Terasaki, O.; Zhao, D.; Pérez-Pariente, J.; Kim, J. M.; Stucky, G. D. *J. Phys. Chem. B* **2002**, *106*, 3118.

62. Liang, Y.; Hanzlik, M.; Anwander, R. *Chem. Commun.* **2005**, 525.

63. Kleitz, F.; Solovyov, L. A.; Anilkumar, G. M.; Choi, S. H.; Ryoo, R. *Chem. Commun.* **2004**, 1536.

64. Sakya, P.; Seddon, J. M.; Templer, R. H.; Mirkin, R. J.; Tiddy, G. J. T. *Langmuir* **1997**, *13*, 3706.

65. Kleitz, F.; Kim, T.-W.; Ryoo, R. *Langumir*, in press.

66. Ryoo, R.; Joo, S. H. *Stud. Surf. Sci. Catal.* **2004**, *148*, 241.

67. Shen, W.; Shi, J.; Chen, H.; Gu, J.; Zhu, Y.; Dong, X. *Chem. Letters* **2005**, *34*, 390.

68. Rossinyol, E.; Arbiol, J.; Peiró, F.; Cornet, A.; Morante, J. R.; Tian, B.; Bo, T.; Zhao, D. *Sensors and Actuors B* **2005**, *109*, 57.

69. Choi, M.; Kleitz, F.; Liu, D.; Lee, H. Y.; Ahn, W.-S.; Ryoo, R. *J. Am. Chem. Soc.* **2005**, *127*, 1924.